Design of IPMSM with Eccentric Rotor and Search Coils for Absolute Position Sensorless Drive

Yong-Cheol Kwon, and Seung-Ki Sul
School of Electrical & Computer Engineering
Seoul National University, Korea
dydcjfe@gmail.com, sulsk@plaza.snu.ac.kr

Noor Aamir Baloch, Shinya Morimoto, and Motomichi Ohto
Energy Conversion Technology Group
Yaskawa Electric Corporation, Japan
Noor.Aamir.Baloch@yaskawa.co.jp,
Shinya.Morimoto@yaskawa.co.jp, Motomichi.Ohto@yaskawa.co.jp

***Abstract*-- In this paper, a design methodology of IPMSM for absolute position sensorless drive is proposed. In conventional researches on the absolute position estimation, initial motion of the rotor was required, which was not allowed in many applications. To eliminate the initial motion, an IPMSM with eccentric rotor with search coils is devised. In the proposed design, the information of the absolute position is included in the voltage signals at the search coils. By measuring the search coil voltages and analyzing them, the absolute position can be estimated without the initial motion of the rotor. The overall performances of the proposed motor design are evaluated by rigorous finite element analyses and experimental tests.**

***Index Terms*—Absolute position sensorless drive, finite element method (FEM), motor design, permanent magnet synchronous machine.**

Nomenclatures

PP	number of pole pairs.
θ_{rm}	rotor position in mechanical angle.
θ_r	rotor position in electrical angle, $PP \cdot \theta_{rm}$.
$\hat{\theta}_{rm}$	estimated value of θ_{rm}.
$\hat{\theta}_r$	estimated value of θ_r.
λ_f	back-EMF constant.
R_s	stator winding resistance.
L_{ds} , L_{qs}	synchronous inductances.
v_{ds}^s , v_{qs}^s	d and q components of stator input voltage in stationary reference frame.
v_{dm}^s , v_{qm}^s	d and q components of search coil voltage in stationary reference frame.
°E	degrees in electrical angle (unit of angle).
°M	degrees in mechanical angle (unit of angle).

I. Introduction

Sensorless control of Interior Permanent Magnet Synchronous Machine (IPMSM) has been developed and widely used for its advantages such as reduced cost and axial length of drive system and enhanced reliability. Sensorless control algorithms can be categorized into two groups: fundamental model based methods [1]-[2] and saliency tracking methods [3]-[5]. Although the former methods show reasonable performance at medium to high speed range, its accuracy of rotor position estimation is degraded at zero to low speed range since the magnitude of back-EMF becomes very small at this range. And, that makes the rotor position estimation vulnerable to disturbances such as inverter nonlinearities and current sensing error. Especially at zero to low speed range, saliency tracking methods [3]-[5] have been used. Since the inductance of IPMSM is clearly determined by the rotor position, the rotor position can be estimated by injecting additional High Frequency (HF) voltage signal and analyzing its resultant HF current ripple.

Despite the development of rotor position estimation technique so far, the estimation of absolute (mechanical) rotor position has been rarely considered. In most conventional researches [1]-[5], rotor position only in electrical angle, not in mechanical angle, was estimated. The following equation addresses the relation between the rotor position in mechanical angle and that in electrical angle.

$$\theta_r = PP \cdot \theta_{rm} . \tag{1}$$

Since θ_r is normally bounded between -180° and 180°, θ_{rm} can't be uniquely determined from the information of θ_r. Although the information regarding θ_r is enough in normal applications which only require the torque/speed control, in some applications such as control of robot arms and machine tools, the absolute rotor position (θ_{rm}) should be identified and controlled. In usual AC motor designs, their inductances are repeated according to the rotor position for every revolution in electrical angle (θ_r=2π), which makes it difficult to identify the absolute rotor position. Thus, the modification of basic motor design is essential for the absolute rotor position estimation.

In references [6]-[7], IPMSM designs with non-uniform winding and asymmetric rotor had been proposed. With the stator and rotor asymmetries, the inductances are not repeated like normal motors anymore, but a little bit modulated according to θ_{rm}. The modulated inductance can be reflected to HF current ripple induced by HF voltage injection, which can be exploited for identifying θ_{rm}. However, in the designs proposed in [6]-[7], the information of the absolute position was measurable only at several distinct positions. And, the rotor had to be aligned to the specific positions to get

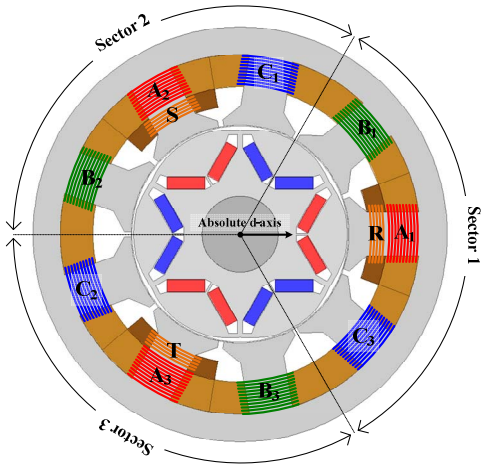

(a) Cross-sectional diagram

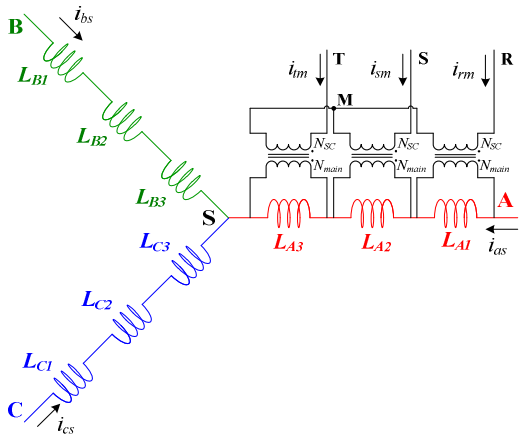

(b) Winding configuration

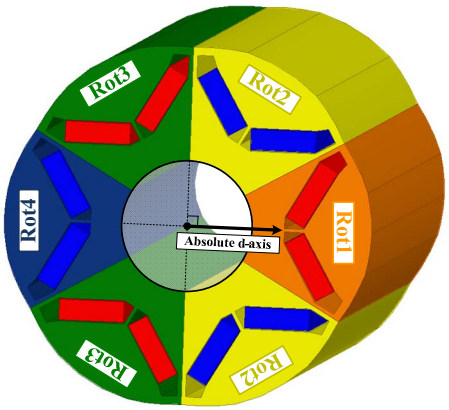

(c) Structure of rotor (assembly of rotor pieces)

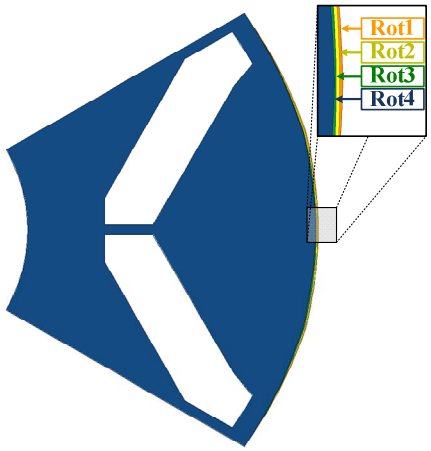

(d) Structure of rotor (overlapped rotor pieces)

Fig. 1. Proposed motor design.

absolute position information. This brought about undesired initial motion of the rotor which was 100°M in [6] and 30°M in [7] in the worst case. In robot and machine tool applications, such a large initial movement of the rotor might be unacceptable.

This paper proposes a design of IPMSM for the estimation of the absolute rotor position without initial motion of the rotor. The proposed design has eccentric rotor and additional search coils wound in A-phase teeth. Injecting HF voltage to the main winding, the voltages measured at the search coils include the information of the absolute position. By analyzing the voltages at search coils, absolute position can be identified without initial motion of the rotor. The effectiveness of the proposed design is verified by analytic approach, finite element analyses, and experiments in sequence.

II. Proposed Method

A. Basic Structure of Proposed Motor

In Fig. 1, overall structure of the proposed motor is shown. There are two windings at the stator: main winding (ABC) that delivers power to the motor and search coil winding (RST) that is used to measure voltage. As shown in Fig. 1(a), there are three sectors according to the rotor position in mechanical angle. In Fig. 1(b), the connection of coils can be seen. In the proposed designs, each phase of the main winding consists of series-connected three 40-turn coils and the three phase windings as linked in Y connection. But three search coils are linked in Y connection and they themselves form a three-phase winding. The search coils work as voltage transformers converting input voltage applied to main winding to another 3-phase voltage. The turn numbers of the main coil and the search coil are denoted as N_{main} and N_{SC}, respectively. The nominal parameters of IPMSM under consideration are listed in Table I.

TABLE I. Specifications of Target IPMSM

Rated power	300 W
Rated speed	3000 r/min
Rated current	2.85 A_{rms}
Number of poles	6 poles
R_s	0.49 Ω
λ_f	0.065 V·s
L_{ds}	6.9 mH
L_{qs}	10.6 mH

In Fig. 1(c)-(d), the structure of the rotor is shown. The rotor consists of the four rotor pieces named as Rot1-Rot4. As shown in Fig. 1(d), the surface of each rotor

$$\begin{bmatrix} \lambda_{as1\_n} \\ \lambda_{bs1\_n} \\ \lambda_{cs1\_n} \\ \cdot \\ \cdot \\ \cdot \\ \lambda_{asPP\_n} \\ \lambda_{bsPP\_n} \\ \lambda_{csPP\_n} \end{bmatrix} = L_n \begin{bmatrix} \cos n\theta_{rm} & k_n \cos n\left(\theta_{rm}-\frac{1}{3PP}\pi\right) & 0 & 0 & 0 & 0 & 0 & 0 & k_n \cos n\left(\theta_{rm}+\frac{1}{3PP}\pi\right) \\ k_n \cos n\left(\theta_{rm}-\frac{1}{3PP}\pi\right) & \cos n\left(\theta_{rm}-\frac{2}{3PP}\pi\right) & k_n \cos n\left(\theta_{rm}-\frac{3}{3PP}\pi\right) & 0 & 0 & 0 & 0 & 0 & 0 \\ 0 & k_n \cos n\left(\theta_{rm}-\frac{3}{3PP}\pi\right) & \cos n\left(\theta_{rm}-\frac{4}{3PP}\pi\right) & \cdot & 0 & 0 & 0 & 0 & 0 \\ 0 & 0 & k_n \cos n\left(\theta_{rm}-\frac{5}{3PP}\pi\right) & \cdot & \cdot & 0 & 0 & 0 & 0 \\ 0 & 0 & 0 & \cdot & \cdot & \cdot & 0 & 0 & 0 \\ 0 & 0 & 0 & 0 & \cdot & \cdot & k_n \cos n\left(\theta_{rm}+\frac{7}{3PP}\pi\right) & 0 & 0 \\ 0 & 0 & 0 & 0 & 0 & \cdot & \cos n\left(\theta_{rm}+\frac{6}{3PP}\pi\right) & k_n \cos n\left(\theta_{rm}+\frac{5}{3PP}\pi\right) & 0 \\ 0 & 0 & 0 & 0 & 0 & 0 & k_n \cos n\left(\theta_{rm}+\frac{5}{3PP}\pi\right) & \cos n\left(\theta_{rm}+\frac{4}{3PP}\pi\right) & k_n \cos n\left(\theta_{rm}+\frac{3}{3PP}\pi\right) \\ k_n \cos n\left(\theta_{rm}+\frac{1}{3PP}\pi\right) & 0 & 0 & 0 & 0 & 0 & 0 & k_n \cos n\left(\theta_{rm}+\frac{3}{3PP}\pi\right) & \cos n\left(\theta_{rm}+\frac{2}{3PP}\pi\right) \end{bmatrix} \begin{bmatrix} i_{as1} \\ i_{bs1} \\ i_{cs1} \\ \cdot \\ \cdot \\ \cdot \\ i_{asPP} \\ i_{bsPP} \\ i_{csPP} \end{bmatrix}. \quad (3)$$

$$\mathbf{L_{abcsn}} = \begin{cases} PP \cdot L_n \begin{bmatrix} \cos a\theta_r & -\frac{1}{2\cos\frac{\pi}{3}a}\cos a\left(\theta_r-\frac{1}{3}\pi\right) & -\frac{1}{2\cos\frac{\pi}{3}a}\cos a\left(\theta_r+\frac{1}{3}\pi\right) \\ -\frac{1}{2\cos\frac{\pi}{3}a}\cos a\left(\theta_r-\frac{1}{3}\pi\right) & \cos a\left(\theta_r-\frac{2}{3}\pi\right) & -\frac{1}{2\cos\frac{\pi}{3}a}\cos a\left(\theta_r+\frac{3}{3}\pi\right) \\ -\frac{1}{2\cos\frac{\pi}{3}a}\cos a\left(\theta_r+\frac{1}{3}\pi\right) & -\frac{1}{2\cos\frac{\pi}{3}a}\cos a\left(\theta_r+\frac{3}{3}\pi\right) & \cos a\left(\theta_r+\frac{2}{3}\pi\right) \end{bmatrix} & \text{for } n = a \cdot PP \\ \begin{bmatrix} 0 & 0 & 0 \\ 0 & 0 & 0 \\ 0 & 0 & 0 \end{bmatrix} & \text{otherwise} \end{cases}. \quad (5)$$

piece is slightly shaved with different depth. This means that each rotor piece has different air-gap between the stator and the rotor. For this reason, the rotor which is an assembly of the rotor pieces enforces a distinctive feature in the inductance. Although an ideal IPMSM has only one 2nd order saliency in electrical angle, the proposed IPMSM has additional 1st order saliency in mechanical angle coming from the shaved rotor. The dimension of the shaving is determined so that self and mutual inductances of the proposed motor have additional sinusoidal component with period of θ_{rm} =2π, i.e., $L_1 \cos(\theta_{rm}+\phi)$.

B. Modeling of Proposed Motor

At first, the effect of the search coils shall be ignored in the analysis. Before considering the connection of coils, each self-inductance of a coil or mutual inductance between coils can be expressed as a function of θ_{rm}. And the inductance can be thought as a sum of many frequency components. For example, self-inductance of A_1 coil in Fig. 1(a) can be expressed as (2).

$$L_{a1a1} = \sum_{n=0}^{\infty} L_n \cos(n\theta_{rm} + \phi_n). \quad (2)$$

Note that n in (2) is the harmonic order based on mechanical angle. Considering magnetic coupling between coils, n^{th} order flux linkages of the coils can be expressed as (3). In (3), there is an assumption that flux linkage of a coil is affected only by the currents flowing through the coil itself and other two coils nearby. In the case of the proposed motor, PP=3 since it is a 6-pole machine. In (3), k_n can be given by (4).

$$k_n = -\frac{1}{2\cos\frac{n}{3PP}\pi}. \quad (4)$$

Considering series connection of coils in each phase and Y connection of ABC phase windings, n^{th} order inductances of ABC phases can be deduced as (5), where a is an arbitrary integer. It is worth noting that only the harmonic inductance with its harmonic number equal to a multiple of PP can be seen from the main winding. The total inductance can be expressed as (6).

$$\mathbf{L_{abcs}} = \mathbf{L_{ls}} + \sum_{\mathbf{n}=0}^{\infty} \mathbf{L_{abcsn}}, \quad (6)$$

where $\begin{bmatrix} \lambda_{as} \\ \lambda_{bs} \\ \lambda_{cs} \end{bmatrix} = \mathbf{L_{abcs}} \begin{bmatrix} i_{as} \\ i_{bs} \\ i_{cs} \end{bmatrix}$.

In the case of an ideal IPMSM, there are only zero and $2PP^{th}$ order inductances, which can be deduced as (7)-(8).

$$\mathbf{L_{abc0}} = PP \cdot L_0 \begin{bmatrix} 1 & -\frac{1}{2} & -\frac{1}{2} \\ -\frac{1}{2} & 1 & -\frac{1}{2} \\ -\frac{1}{2} & -\frac{1}{2} & 1 \end{bmatrix}. \quad (7)$$

$$\mathbf{L_{abc2PP}} = PP \cdot L_{2PP} \begin{bmatrix} \cos 2\theta_r & \cos 2\left(\theta_r-\frac{\pi}{3}\right) & \cos 2\left(\theta_r+\frac{\pi}{3}\right) \\ \cos 2\left(\theta_r-\frac{\pi}{3}\right) & \cos 2\left(\theta_r+\frac{\pi}{3}\right) & \cos 2\theta_r \\ \cos 2\left(\theta_r+\frac{\pi}{3}\right) & \cos 2\theta_r & \cos 2\left(\theta_r-\frac{\pi}{3}\right) \end{bmatrix}. \quad (8)$$

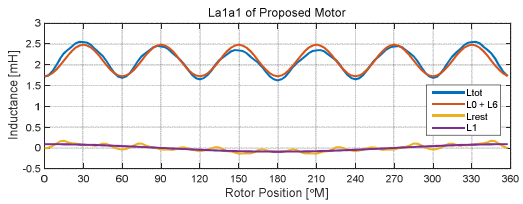

(a) L_{ala1} according to absolute rotor position

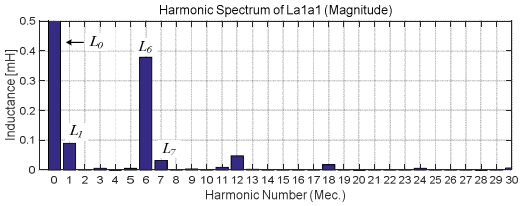

(b) Harmonic spectrum of L_{ala1}

Fig. 2. Self-inductance of A_1 coil, L_{ala1} (FEM).

$$\mathbf{L_{abcs}} = \mathbf{L_{ls}} + \mathbf{L_{abcs0}} + \mathbf{L_{abcs2PP}} = \begin{bmatrix} L_{ls}+L_A+L_B\cos 2\theta_r & -\frac{1}{2}L_A+L_B\cos 2\left(\theta_r-\frac{\pi}{3}\right) & -\frac{1}{2}L_A+L_B\cos 2\left(\theta_r+\frac{\pi}{3}\right) \\ -\frac{1}{2}L_A+L_B\cos 2\left(\theta_r-\frac{\pi}{3}\right) & L_{ls}+L_A+L_B\cos 2\left(\theta_r+\frac{\pi}{3}\right) & -\frac{1}{2}L_A+L_B\cos 2\theta_r \\ -\frac{1}{2}L_A+L_B\cos 2\left(\theta_r+\frac{\pi}{3}\right) & -\frac{1}{2}L_A+L_B\cos 2\theta_r & L_{ls}+L_A+L_B\cos 2\left(\theta_r-\frac{\pi}{3}\right) \end{bmatrix}. \quad (9)$$

The total inductance of an ideal IPMSM can be expressed as (9), where $L_A = PP \cdot L_0$ and $L_B = PP \cdot L_{2PP}$. Eq. (9) is a general inductance model of an ideal IPMSM that is addressed in many textbooks [8]-[9].

Considering the effect of the search coils, the voltages at the search coils can be derived as follows. Since the search coil is only for voltage measurement, there is almost zero current at the search coil ($\mathbf{i_{rstm}} = 0$). Then n^{th} order components of flux linkages of A-phase main coils can be expressed as (10).

$$\begin{bmatrix} \lambda_{as1n} \\ \lambda_{as2n} \\ \lambda_{as3n} \end{bmatrix} = \left(\mathbf{L_{asn\_1}} + \mathbf{L_{asn\_2}}\right) \cdot \begin{bmatrix} i_{as} \\ i_{bs} \\ i_{cs} \end{bmatrix}, \quad (10)$$

where

$$\mathbf{L_{asn\_1}} = L_n \begin{bmatrix} \cos n\theta_{rm} & 0 & 0 \\ \cos n\left(\theta_{rm}-\frac{6}{9}\pi\right) & 0 & 0 \\ \cos n\left(\theta_{rm}+\frac{6}{9}\pi\right) & 0 & 0 \end{bmatrix},$$

$$\mathbf{L_{asn\_2}} = k_n L_n \begin{bmatrix} 0 & \cos n\left(\theta_{rm}-\frac{1}{9}\pi\right) & \cos n\left(\theta_{rm}+\frac{1}{9}\pi\right) \\ 0 & \cos n\left(\theta_{rm}-\frac{7}{9}\pi\right) & \cos n\left(\theta_{rm}-\frac{5}{9}\pi\right) \\ 0 & \cos n\left(\theta_{rm}+\frac{5}{9}\pi\right) & \cos n\left(\theta_{rm}+\frac{7}{9}\pi\right) \end{bmatrix}.$$

The flux linkages of A-phase main coils can be expressed as (11).

$$\begin{bmatrix} \lambda_{as1} \\ \lambda_{as2} \\ \lambda_{as3} \end{bmatrix} = \frac{1}{3}\begin{bmatrix} L_{ls} \\ L_{ls} \\ L_{ls} \end{bmatrix} i_{as} + \sum_{n=0}^{\infty}\left(\mathbf{L_{asn\_1}} + \mathbf{L_{asn\_2}}\right) \cdot \begin{bmatrix} i_{as} \\ i_{bs} \\ i_{cs} \end{bmatrix} + \frac{1}{3}\lambda_f \begin{bmatrix} \cos\theta_r \\ \cos\theta_r \\ \cos\theta_r \end{bmatrix}. \quad (11)$$

In Fig. 1(a), RST coils would be magnetically well-coupled with A-phase coils. So, flux linkages of the search coils in RST coordinate plane can be deduced as (12).

$$\begin{bmatrix} \lambda_{rm} \\ \lambda_{sm} \\ \lambda_{tm} \end{bmatrix} = \frac{N_{SC}}{N_{main}}\left(\begin{bmatrix} \lambda_{as1} \\ \lambda_{as2} \\ \lambda_{as3} \end{bmatrix} - \frac{1}{3}\begin{bmatrix} L_{ls} \\ L_{ls} \\ L_{ls} \end{bmatrix} i_{as}\right) = \frac{1}{3}\lambda_f \frac{N_{SC}}{N_{main}}\begin{bmatrix} \cos\theta_r \\ \cos\theta_r \\ \cos\theta_r \end{bmatrix} + \frac{N_{SC}}{N_{main}}\sum_{n=0}^{\infty}\left(\mathbf{L_{asn\_1}} + \mathbf{L_{asn\_2}}\right) \cdot \begin{bmatrix} i_{as} \\ i_{bs} \\ i_{cs} \end{bmatrix}. \quad (12)$$

Transforming (12) into dqn coordinate plane, (13) can be obtained.

$$\begin{bmatrix} \lambda^s_{dm} \\ \lambda^s_{qm} \\ \lambda^s_{nm} \end{bmatrix} = \frac{1}{3}\lambda_f \frac{N_{SC}}{N_{main}}\begin{bmatrix} 0 \\ 0 \\ \cos\theta_r \end{bmatrix} + \frac{N_{SC}}{N_{main}}\sum_{n=0}^{\infty}\mathbf{T_{dqn}}\left(\mathbf{L_{asn\_1}} + \mathbf{L_{asn\_2}}\right)\mathbf{T_{dqn}}^{-1}\begin{bmatrix} i^s_{ds} \\ i^s_{qs} \\ i^s_{ns} \end{bmatrix}. \quad (13)$$

In (13), $\mathbf{T_{dqn}}$ indicates the transformation matrix defined as (14).

$$\mathbf{T_{dqn}} = \frac{2}{3}\begin{bmatrix} 1 & -\frac{1}{2} & -\frac{1}{2} \\ 0 & \frac{\sqrt{3}}{2} & -\frac{\sqrt{3}}{2} \\ \frac{1}{2} & \frac{1}{2} & \frac{1}{2} \end{bmatrix}. \quad (14)$$

After some algebraic manipulation, $\mathbf{T_{dqn}}\left(\mathbf{L_{asn\_1}} + \mathbf{L_{asn\_2}}\right)\mathbf{T_{dqn}}^{-1}$ in (13) can be derived as (15).

$$\mathbf{T_{dqn}}\left(\mathbf{L_{asn\_1}} + \mathbf{L_{asn\_2}}\right)\mathbf{T_{dqn}}^{-1} = \begin{cases} \begin{bmatrix} 0 & 0 & 0 \\ 0 & 0 & 0 \\ 0 & 0 & 0 \end{bmatrix} & \text{for } n = 3a \\ L_n \begin{bmatrix} \frac{3}{2}\cos n\theta_{rm} & -\frac{\sqrt{3}}{2}\tan\frac{1}{9}n\pi\cos\left(n\theta_{rm}-\frac{\pi}{2}\right) & 0 \\ \frac{3}{2}\sin n\theta_{rm} & -\frac{\sqrt{3}}{2}\tan\frac{1}{9}n\pi\sin\left(n\theta_{rm}-\frac{\pi}{2}\right) & 0 \\ 0 & 0 & 0 \end{bmatrix} & \text{for } n = 3a+1 \\ L_n \begin{bmatrix} \frac{3}{2}\cos n\theta_{rm} & -\frac{\sqrt{3}}{2}\tan\frac{1}{9}n\pi\cos\left(n\theta_{rm}-\frac{\pi}{2}\right) & 0 \\ -\frac{3}{2}\sin n\theta_{rm} & \frac{\sqrt{3}}{2}\tan\frac{1}{9}n\pi\sin\left(n\theta_{rm}-\frac{\pi}{2}\right) & 0 \\ 0 & 0 & 0 \end{bmatrix} & \text{for } n = 3a+2 \end{cases}, \quad (15)$$

where a is an arbitrary integer.

Self-inductance of A_1 coil, L_{ala1}, of the proposed motor according to the rotor position in mechanical angle which is calculated by FEM simulation is shown in Fig. 2. In Fig. 2(a), L_{tot} indicates the total inductance. L_0 and L_6 indicate zero and 6th order inductances, respectively. And

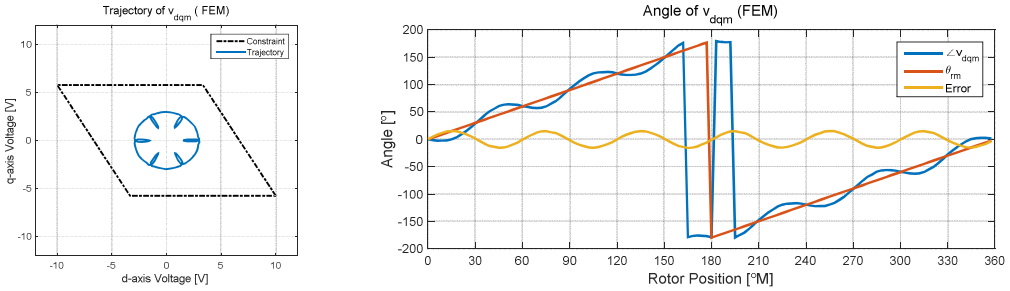

(a) From FEM simulation

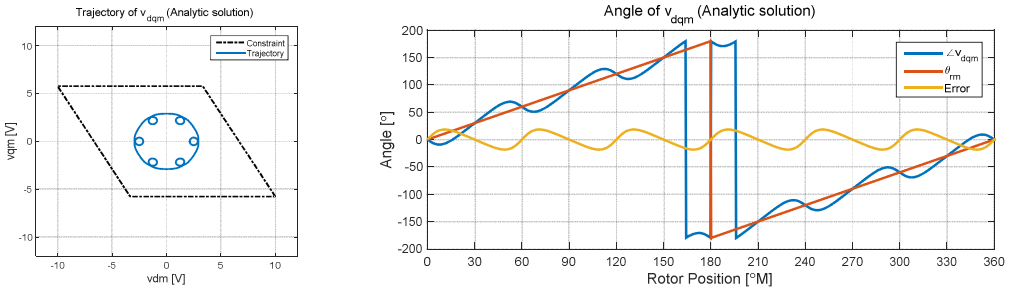

(b) From analytic solution in (19)

Fig. 3. Trajectory and angle of v^s_{dqm}.

$$\begin{bmatrix}\lambda^s_{dm}\\ \lambda^s_{qm}\end{bmatrix}=\sum_{n=1,7}\left\{\begin{matrix}K_1L_n\left(L_\Sigma-L_\Delta\cos 2\theta_r\right)\begin{bmatrix}\cos n\theta_{rm} & 0\\ \sin n\theta_{rm} & 0\end{bmatrix}+K_2L_nL_\Delta\sin 2\theta_r\begin{bmatrix}\cos\left(n\theta_{rm}-\frac{\pi}{2}\right) & 0\\ \sin\left(n\theta_{rm}-\frac{\pi}{2}\right) & 0\end{bmatrix}\\ -K_1L_nL_\Delta\sin 2\theta_r\begin{bmatrix}0 & \cos n\theta_{rm}\\ 0 & \sin n\theta_{rm}\end{bmatrix}-K_2L_n\left(L_\Sigma+L_\Delta\cos 2\theta_r\right)\begin{bmatrix}0 & \cos\left(n\theta_{rm}-\frac{\pi}{2}\right)\\ 0 & \sin\left(n\theta_{rm}-\frac{\pi}{2}\right)\end{bmatrix}\end{matrix}\right\}\left(\begin{bmatrix}\lambda^s_{ds}\\ \lambda^s_{qs}\end{bmatrix}-\lambda_f\begin{bmatrix}\cos\theta_r\\ \sin\theta_r\end{bmatrix}\right). \quad (17)$$

L_{rest} is defined as $L_{rest}=L_{tot}-(L_0+L_6)$. Although L_{tot} mainly consists of L_0 and L_6, there is low frequency component in L_{tot}. That component is L_1 which is intendedly induced by the shaving of the rotor surface. From Fig. 2(b) which is the result of Fast Fourier Transform (FFT) of L_{a1a1}, it can be seen that 7th harmonic is also induced by the shaving of the rotor. It can be thought that L_1 and L_7 came from the shaving of the rotor. Other additional harmonics are so small that they are neglected in this analysis.

As expressed in (5), $\mathbf{L}_{\mathbf{abcsn}}$ becomes zero if n is not a multiple of PP. In the case of the proposed motor where $PP=3$, '1' and '7' are not a multiple of PP. For this reason, L_1 and L_7 can't be seen from main terminals. But they can be seen from search coil terminals. Zero and 6th order components in inductances have no impact on the search coil voltage expressed in (15) since they are in the case of $n=3a$. But L_1 and L_7 affect the search coil voltage since they are in the case of $n=3a+1$ in (15). Assuming that L_1 and L_7 components are added to an ideal IPMSM which only contains L_0 and L_6, the search coil voltage can be expressed as (16).

$$\begin{bmatrix}\lambda^s_{dm}\\ \lambda^s_{qm}\\ \lambda^s_{nm}\end{bmatrix}=\frac{1}{3}\lambda_f\frac{N_{SC}}{N_{main}}\begin{bmatrix}0\\ 0\\ \cos\theta_r\end{bmatrix}+\frac{N_{SC}}{N_{main}}\sum_{n=1,7}\mathbf{T}_{\mathbf{dqn}}\left(\mathbf{L}_{\mathbf{asn\_1}}+\mathbf{L}_{\mathbf{asn\_2}}\right)\mathbf{T}_{\mathbf{dqn}}^{-1}\begin{bmatrix}i^s_{ds}\\ i^s_{qs}\\ i^s_{ns}\end{bmatrix}. \quad (16)$$

Neglecting n-axis components that is not used, (16) can be simplified as (17), where K_1 and K_2 are defined as (18).

$$K_1=\frac{3}{2}\frac{N_{SC}}{N_{main}}\frac{1}{L_{ds}L_{qs}}$$
$$K_2=\frac{\sqrt{3}}{2}\tan\frac{1}{9}\pi\frac{N_{SC}}{N_{main}}\frac{1}{L_{ds}L_{qs}}. \quad (18)$$

Then the search coil voltage in dq coordinate plane is represented as (19).

$$\begin{bmatrix}v^s_{dm}\\ v^s_{qm}\end{bmatrix}=\frac{d}{dt}\begin{bmatrix}\lambda^s_{dm}\\ \lambda^s_{qm}\end{bmatrix}=\sum_{n=1,7}\left\{\begin{matrix}K_1L_n\left(L_\Sigma-L_\Delta\cos 2\theta_r\right)\begin{bmatrix}\cos n\theta_{rm}\\ \sin n\theta_{rm}\end{bmatrix}\\ +K_2L_nL_\Delta\sin 2\theta_r\begin{bmatrix}\cos\left(n\theta_{rm}-\frac{\pi}{2}\right)\\ \sin\left(n\theta_{rm}-\frac{\pi}{2}\right)\end{bmatrix}\end{matrix}\right\}v^s_{ds} \quad (19)$$

In the derivation of (19), θ_{rm} is assumed as a constant. And v^s_{qs} is neglected since the injection voltage is applied only at d-axis ($v^s_{qs}=0$) in the absolute position estimation process. The blue-colored term in (19) clearly contains the information of the rotor position in its angle.

In Fig. 3, trajectory and angle of v^s_{dqm} according to the absolute position calculated from the analytic solution

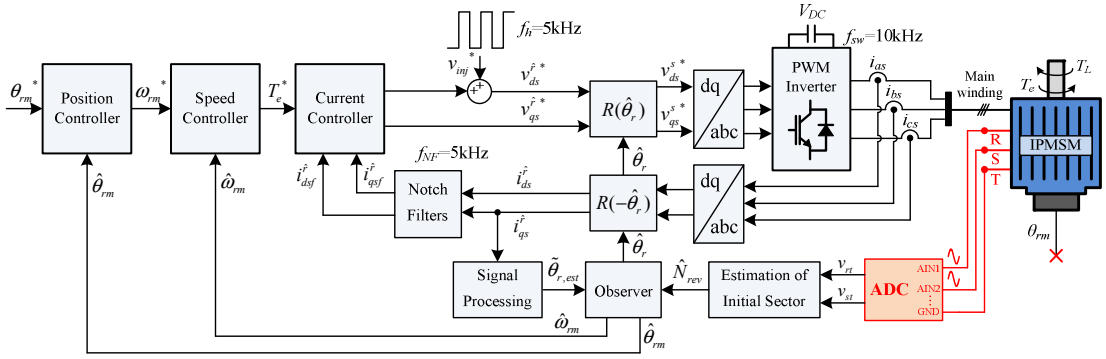

Fig. 4. Block diagram of proposed absolute position sensorless drive system.

and from FEM are shown. In the computation, v_{ds}^s is set as 200V. Trajectory and angle of v_{dqm}^s calculated from (19) well matches to FEM results. This proves the validity of Eq. (19). Small difference between Fig. 3(a) and (b) comes from the error in the model in (3) and that harmonic inductances other than L_1 and L_7 are neglected in (19). The clear correlation between the angle of v_{dqm}^s and θ_{rm} visualized in Fig. 3 can be utilized in the estimation of the absolute position.

C. Estimation of Absolute Position

In Fig. 4, block diagram of the proposed absolute position sensorless drive system including the configuration of search coil voltage measurement is shown. Basic sensorless control algorithm is based on the square-wave injection method [5] with some modification. As specified in (19), because only rotary (dq) components carry the information of the absolute rotor position, line-to-line voltages are enough for the estimation of the absolute position. Thus only v_{rt} and v_{st} are directly measured by Analog to Digital Converter (ADC) of control board. From the measured v_{rt} and v_{st}, $\mathbf{v}_{\mathbf{dqm}}^{\mathbf{s}}$ can be calculated by (20).

$$\mathbf{v}_{\mathbf{dqm}}^{\mathbf{s}} = \begin{bmatrix} v_{dm}^s \\ v_{qm}^s \end{bmatrix} = \begin{bmatrix} \frac{2}{3} & -\frac{1}{3} \\ 0 & \frac{1}{\sqrt{3}} \end{bmatrix} \begin{bmatrix} v_{rt} \\ v_{st} \end{bmatrix} \tag{20}$$

For the measurement of v_{rt} and v_{st}, voltage is injected at d-axis of the main winding in stationary reference frame. Because v_{rt} and v_{st} are proportional to v_{ds}^s, v_{rt} and v_{st} can be directly sampled by the ADC while v_{ds}^s is high. Since ADC has an input range, v_{rt} and v_{st} should be properly limited within the input range of ADC. Using an ADC with ±10V input range, the constraints of v_{dm}^s and v_{qm}^s can be expressed as (21).

$$\begin{aligned} -\sqrt{3}v_{dm}^s - \frac{20}{\sqrt{3}} \le v_{qm}^s \le -\sqrt{3}v_{dm}^s + \frac{20}{\sqrt{3}} \\ -\frac{10}{\sqrt{3}} \le v_{qm}^s \le \frac{10}{\sqrt{3}} \end{aligned} \tag{21}$$

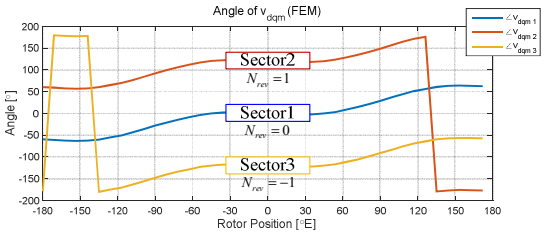

Fig. 5. $\angle v_{dqm}^s$ according to rotor position (FEM).

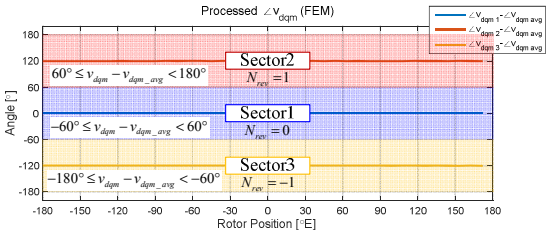

Fig. 6. $\angle v_{dqm}^s - \angle v_{dqm\_avg}^s$ according to rotor position (FEM).

The constraint specified in (21) has a parallelogram shape in dq coordinate plane as shown in Fig. 3.

From the measured v_{rt} and v_{st}, initial absolute position can be estimated. The absolute rotor position can be expressed as (22).

$$\theta_{rm} = \frac{1}{PP}\left(\theta_r + 2\pi \cdot N_{rev}\right). \tag{22}$$

N_{rev} in (22) stands for a counting number of rotor revolution in electrical angle. Transforming variables in (22) to estimated values, can be deduced as (23).

$$\hat{\theta}_{rm} = \frac{1}{PP}\left(\hat{\theta}_r + 2\pi \cdot \hat{N}_{rev}\right). \tag{23}$$

In a basic sensorless control, only $\hat{\theta}_r$ can be estimated. In order to get $\hat{\theta}_{rm}$, $\hat{N}_{rev}$ should be estimated. In Fig. 5, the voltage angle, $\angle v_{dqm}^s$, according to the rotor position in electrical angle is shown, which is constructed from $\angle v_{dqm}^s$ in Fig. 3(a). It is clear that $\angle v_{dqm}^s$ of three sectors are 120° apart from each other. In order to estimate $\hat{N}_{rev}$, first of all, Look Up Table (LUT) data of $\angle v_{dqm\ avg}(\theta_r)$ should be implemented by (24).

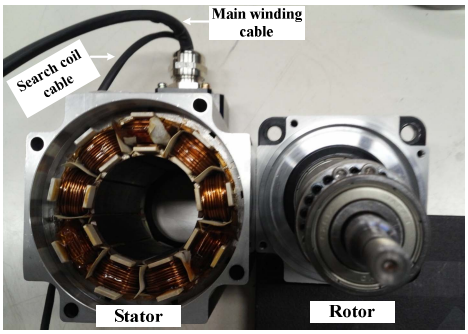

Fig. 7. Contructed prototype motor.

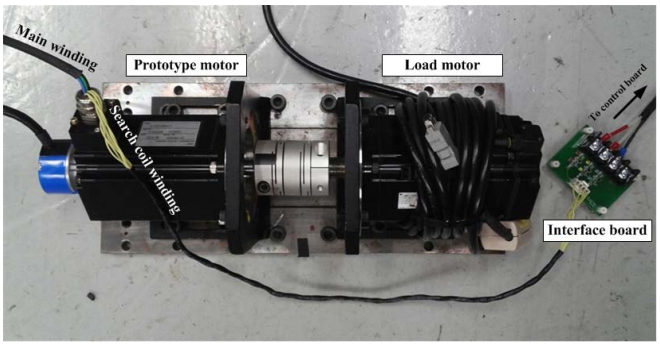

Fig. 8. Motor-Generator set.

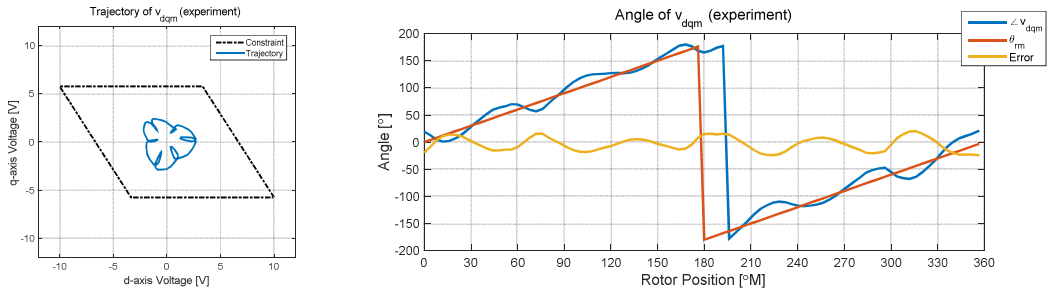

Fig. 9. Trajectory and angle of v_{dqm}^{s} (Exp.).

$$\angle v_{dqm\,avg}(\theta_r) = \frac{\angle v_{dqm1}(\theta_r) + \left(\angle v_{dqm2}(\theta_r) - \frac{2}{3}\pi\right) + \left(\angle v_{dqm3}(\theta_r) + \frac{2}{3}\pi\right)}{3}. \quad (24)$$

Note that $\angle v_{dqm\,avg}(\theta_r)$ is calculated from offline test. Subtracting $\angle v_{dqm\,avg}(\theta_r)$ from $\angle v_{dqm}^{s}$ in Fig. 5, Fig. 6 can be derived. If the rotor is in sector 1, $-60° \le v_{dqm} - v_{dqm\_avg} < 60°$. If the rotor is in sector 2, $60° \le v_{dqm} - v_{dqm\_avg} < 180°$. If the rotor is in sector 3, $-180° \le v_{dqm} - v_{dqm\_avg} < -60°$. From this feature, $\hat{N}_{rev}$ can be estimated by (25).

$$\hat{N}_{rev} = \text{round}\left(\frac{\text{BOUND\_PI}\left(\angle v_{dqm} - \angle v_{dqm\,avg}(\hat{\theta}_r)\right)}{\frac{2}{3}\pi}\right), \quad (25)$$

where BOUND_PI(*) stands for variable '*' is bounded between $-\pi$ to π.

In Fig. 6, $\angle v_{dqm}^{s} - \angle v_{dqm\,avg}(\theta_r)$ is represented as straight lines because it comes from FEM result, which has no measurement error, manufacturing tolerance, no inverter nonlinearity, and etc. In experiment, however, $\angle v_{dqm}^{s} - \angle v_{dqm\,avg}(\theta_r)$ can vary according to θ_r. Fortunately, in this case, there is ±60° error margin in $\angle v_{dqm}^{s} - \angle v_{dqm\,avg}(\theta_r)$.

III. Experimental Results

The proposed motor design described in Fig. 1 is constructed as a prototype, which is shown in Fig. 7. In Fig. 8, Motor-Generator set for experimental test is shown. In addition to main winding cable, there is search coil cable coming out from the prototype motor. The search coil voltage signal directly goes to the control board.

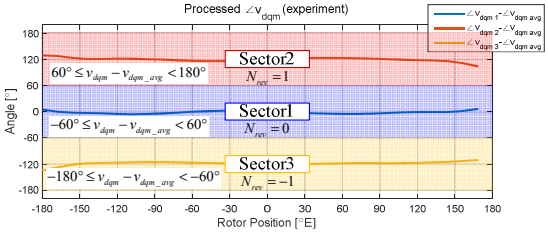

Fig. 10. $\angle v_{dqm}^{s} - \angle v_{dqm\_avg}^{s}$ according to rotor position (Exp.).

In Fig. 9, trajectory and angle of v_{dqm}^{s} obtained from experiment are shown. Compared with the FEM result in Fig. 3(a), the experimental result in Fig. 10 is a little bit distorted. But as shown in Fig. 10, the processed angle of v_{dqm}^{s} has very small error, which guarantees the feasibility of the absolute position estimation algorithm in (25).

In Fig. 11, initial absolute position estimation at various initial positions is demonstrated. At initial startup with signal injection sensorless control, $\hat{N}_{rev}$ is assumed as zero. In every case, 300ms is spent for taking many samples of v_{rt} and v_{st} to calculate their mean values. Because the environment of the voltage measurement can be noisy, it is required to use mean values of v_{rt} and v_{st} for the calculation of $\angle v_{dqm}$. This time period can be tuned according to experimental environment. After 300ms, $\hat{N}_{rev}$ can be obtained by (25). Then, the absolute position can be estimated by (23). After absolute position is estimated, it is programmed to align the rotor to absolute zero by position control. $Flag_{APE}$ in the figure is the flag indicating that the absolute position

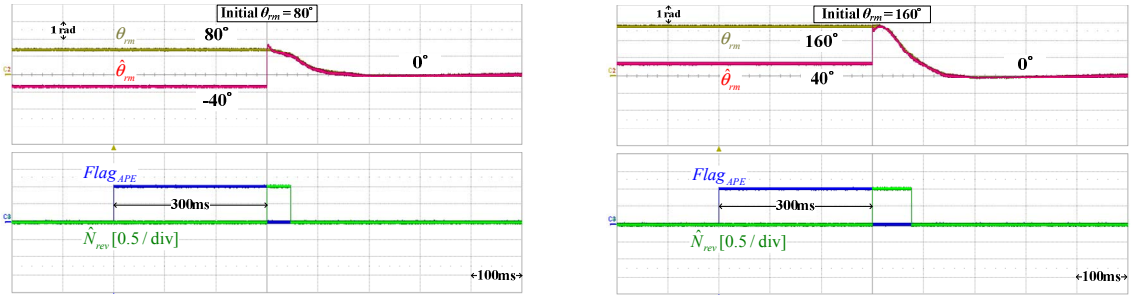

(a) Initial rotor position = 80°M

(b) Initial rotor position = 160°M

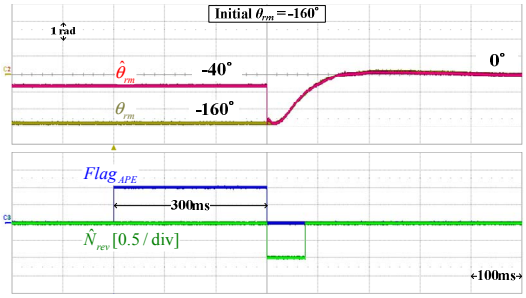

(c) Initial rotor position = -160°M

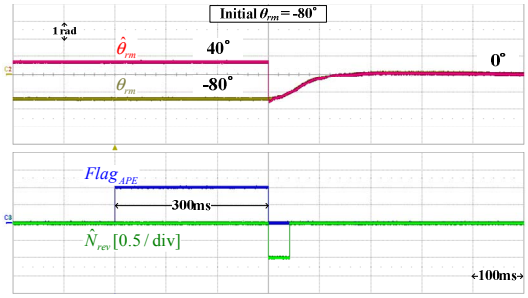

(d) Initial rotor position = -80°M

Fig. 11. Estimation of initial absolute rotor position (Exp.).

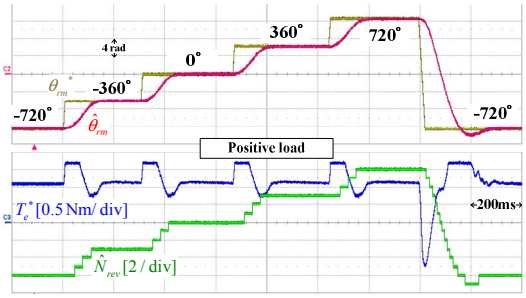

(a) Positive load (T_L>0)

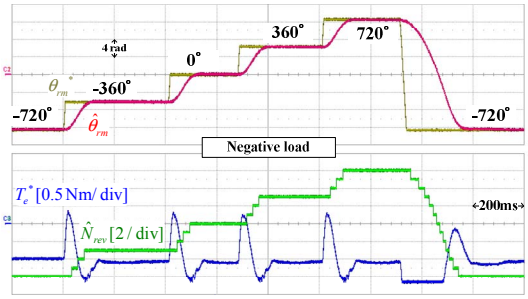

(b) Negative load (T_L<0)

Fig. 12. Control of absolute rotor position (Exp.).

estimation algorithm is running. Regardless of initial position, the absolute rotor position is estimated without any failure in all cases.

Fig. 12 shows the control performance of the absolute position with various load conditions after the identification of initial rotor position shown in Fig. 11. Regardless of load condition, the absolute rotor position is well regulated to its command.

IV. Conclusions

In this paper, an IPMSM design with an eccentric rotor and search coils for absolute position sensorless drive has been proposed. The rotor eccentricity realized by shaved rotor surface induces 1st order inductance in mechanical angle, which is utilized in the absolute position estimation. It has been fully analyzed that the 1st order inductance does not affect the basic inductance seen from the main terminals, but only affects the voltage at the search coils. From the measured voltage at the search coil under signal injection, initial absolute position can be estimated without any initial motion of the rotor. The effectiveness of the proposed IPMSM design is verified by FEM simulations and experiments.

References

[1] N. Matsui, "Sensorless PM brushless DC motor drives," *IEEE Trans. Industrial Electronics*, vol. IE-43, pp. 300-308, Mar. 1996.

[2] Z. Chen, M. Tomita, S. Doki, and S. Okuma, "An extended electromotive force model for sensorless control of interior permanent-magnet synchronous motors," *IEEE Trans. Ind. Electron.*, vol. 50, no. 2, pp. 288-295, Apr. 2003.

[3] P. L. Jansen and R. D. Lorenz, "Transducerless position and velocity estimation in induction and salient AC machines, " *IEEE Trans. Ind. Appl.*, vol. 31, no. 2, pp. 240-247, Mar./ Apr. 1995.

[4] J. I. Ha, and S. K. Sul, "Sensorless field-orientation control of an induction machine by high-frequency signal injection," *IEEE Trans. Ind. Appl.*, vol. 35, no. 1, pp. 45-51, Jan./Feb. 1999.

[5] Y. D. Yoon, S. K. Sul, S. Morimoto, and K. Ide, "High bandwidth sensorless algorithm for AC machines based on square-wave-type voltage injection," *IEEE Trans. Ind. Appl.*, vol. 47, no. 3, pp. 1361-1370, May/Jun. 2011.

[6] Y. C. Kwon, S. K. Sul, N. A. Baloch, S. Murakami, S. Morimoto, "Design and control of IPMSM sensorless drive for mechanical rotor position estimation capability," *Emerging and Selected Topics in Power Electronics, IEEE Journal of* , vol. 2, no. 2, pp. 152-158, June 2014.

[7] Y. C. Kwon, S. K. Sul, N. A. Baloch, S. Murakami, S. Morimoto, "Improved design of IPMSM for sensorless drive with absolute rotor position estimation capability," *Sensorless Control for Electrical Drives (SLED), 2014 IEEE 5th International Symposium on*, pp.1-6, 17-18 May 2014.

[8] D. Novotny and T. Lipo, Vector Control and Dynamics of AC Drives, Oxford: Clarendon Press, 1996, Chapter 2.

[9] S. K. Sul, Control of Electric Machine Drive Systems, John Wiley & Sons, 2011, Chapter 3.